Environmental Science and Pollution Research (2023) 30:72160–72170
https://doi.org/10.1007/s11356-023-27544-7

RESEARCH ARTICLE

Recycling of phosphate tailings for an efficient hydroxyapatite-based adsorbent to immobilize heavy metal cations

Shanshan Wu[1,2] · Yizhang Liu[1] · Lihai Shang[1] · Wangwang Zhou[1] · Yuyang Li[3] · Jing Sun[1] · Jianqiu Li[4] · Hui Long[4] · Zengping Ning[1] · Chengshuai Liu[1]

Received: 19 December 2022 / Accepted: 6 May 2023 / Published online: 11 May 2023

Abstract

Hydroxyapatite (HAP) is a promising adsorbent for immobilizing heavy metals in soil and water. However, the preparation and modification of HAP from pure chemicals increases its cost and limits its large-scale practical application. In this study, a hydroxyapatite-based adsorbent (HAP_{PT}) was prepared from phosphate tailing produced in the phosphorus industry to sequester Pb, Cd and Zn from solution. The results showed that HAP_{PT} was composed of HAP and MgO, with a surface area of 27.74 m^2/g. The kinetics studies showed that most Pb and Cd were removed from the initial solution in 4 h and the adsorption of Zn increased with increasing contact time. Metals presented higher adsorption capacities at 35 °C than that at 25 °C. The adsorption isotherms showed that HAP_{PT} presented high adsorption capacities for Pb, Cd and Zn in mono-metal solutions. The adsorption capacity of Cd at pH 6 was higher than that at pH 3, but the adsorption for Pb and Zn was similar at both pHs. HAP_{PT} has selectivity for Pb in Pb–Cd-Zn multi-metals solution, and competitive adsorption reduced the adsorption quantity by 53%, 93% and 79% for Pb, Cd and Zn, respectively. The combined results of TEM-EDS, XRD and XPS showed that Pb was immobilized by forming phosphates due to the dissolution of HAP, whereas Cd and Zn were immobilized by forming hydroxide precipitates resulting from the function of MgO in HAP_{PT}. The results of this study provided an efficient adsorbent for the removal of heavy metals in solution and provided a new perspective on the recycling of phosphate tailings in the phosphorus industry.

Keywords Hydroxyapatite · Heavy metals · Immobilization · Soil amendment · Solid waste

Introduction

Mining activities of nonferrous metals result in serious contamination of heavy metals (HMs) in the surrounding soils and water (Vareda et al. 2019; Kan et al. 2021). In the past decade, an increasing number of mines, particularly small-scale mines, have been closed to support environmental protection (Cidu et al. 2012). These actions left large amounts of abandoned mine sites that need to be remediated. Among these, Pb−Zn mine sites present significant accumulation of Pb, Zn and Cd in soils, and mine drainage is widespread and threatens the safety of eco-environmental systems and communities (e.g., Marzouk et al. 2013; Liu et al. 2018a; Ayari et al. 2023). Therefore, it is imperative to take appropriate techniques to contain the diffusion of HMs from abandoned mine sites.

Adsorption is one of the most effective and economical strategies to sequester metals in contaminated soils and water (Bolan et al. 2014; Tian et al. 2019; Li et al. 2022b).

Responsible Editor: Tito Roberto Cadaval Jr

✉ Yizhang Liu
liuyizhang@mail.gyig.ac.cn

[1] State Key Laboratory of Environmental Geochemistry, Institute of Geochemistry, Chinese Academy of Sciences, Guiyang 550081, China

[2] University of Chinese Academy of Sciences, Beijing 100049, China

[3] Department of Building Environment and Energy Engineering, The Hong Kong Polytechnic University, Hong Kong, China

[4] Guizhou Chanhen Chemical Corporation, Fuquan 550599, China

Numerous studies have tried to develop adsorbents with both high efficiency and low cost for the removal of metals from solution (Lee et al. 2013; Fang et al. 2017; Tian et al. 2019; Azhar et al. 2022). Recently, hydroxyapatite ($Ca_{10}(PO_4)_6(OH)_2$, HAP) has become a promising material for the immobilization of heavy metals in water and soil because of its high reactivity, low solubility and redox stability (Ibrahim et al. 2020; Nayak and Bhushan 2021; Amenaghawon et al. 2022). To improve the adsorption performance, different pure hydroxyapatite and hydroxyapatite composites were prepared by precipitation/hydrothermal methods in previous studies (Ivanets et al. 2019; Ashrit et al. 2020; Sawada et al. 2021; Yang et al. 2022). For instance, Li et al. (2017) prepared HAP with different surface areas and evaluated their efficiency in the removal of Pb and Cd. Yang et al. (2022) synthesized Fe-doped HAP to improve its ability to immobilize Pb, Cd and As simultaneously. These works improved the adsorption efficiency of HAP, but the high cost of pure chemicals such as H_3PO_4 and $Ca(NO_3)_2$ hindered the large-scale application of HAP.

Comparatively, preparing hydroxyapatite-based adsorbents from cost-friendly raw materials such as solid waste is of increasing concern. For example, researchers prepared hydroxyapatite from flue gas desulphurization gypsum that from coal-fired power plants, and demonstrated that it can effectively immobilize Pb, Cd and Cu in solution and soil (Yan et al. 2014; Liu et al. 2018b). Foroutan et al. (2021) studied the removal of Cd from wastewater by hydroxyapatite prepared from chicken bones (femur and beak) and fishbones and proposed that it is an inexpensive and eco-friendly choice. However, little attention has been given to the recycling of phosphate tailings to prepare hydroxyapatite-based adsorbents. As a byproduct of the floating of phosphate rock, phosphate tailing is one of the largest solid wastes in the phosphorus industry due to the low grade of natural phosphate rocks (Luo et al. 2017; Amar et al. 2022). Hence, recycling phosphate tailing has great environmental significance for green and sustainable development. Interestingly, phosphate tailings have chemical composition similar to those of natural phosphate rocks, commonly composed of carbonates, fluorapatite and quartz (Moukannaa et al. 2018; Gu et al. 2022). This suggested that phosphate tailing could be an alternative source of Ca and P to prepare hydroxyapatite.

Therefore, in the present study, we aimed to extract PO_4^{3-} and Ca^{2+} from phosphate tailings as precursors to prepare hydroxyapatite-based adsorbent. Then, to investigate the physicochemical properties of the prepared adsorbent and to evaluate its performance for the sequestration of the heavy metal cations Pb, Cd and Zn from solution. The objective of this study is to develop an efficient and cost-friendly adsorbent from recycling phosphate tailings to sequester heavy metal cations.

Materials and methods

Preparation of hydroxyapatite from phosphate tailing

The raw phosphate tailings from the flotation of natural phosphate rocks in this study were provided by Guizhou Chanhen Chemical Corporation from southwest China. The precipitation method was applied in this study to synthesize hydroxyapatite, which was optimized based on a previous study (Asri et al. 2010). Briefly, the tailings were dried at 30 °C and ground to pass through a 100-mesh sieve. The sieved tailings were reacted in 1 mol/L HNO_3 at a solid to liquid ratio of 1:15 by vigorously stirring for 30 min to extract Ca^{2+} and PO_4^{3-}. Then, the solution was filtered through a 0.5 µm filter, and the filtrate was collected and adjusted to pH 10 by concentrated $NH_3{\cdot}H_2O$. The precipitate was collected and dried at 100 °C for 8 h and then heated in a muffle furnace at 800 °C for 1 h. The final solid powders were collected and used for the experiment.

Batch experiments for adsorption of heavy metals

The chemical reagents used in this study were of analytical grade. Stock solutions of Pb, Cd and Zn (1 g/L) were prepared from $Pb(NO_3)_2$, $Cd(NO_3)_2$ and $Zn(NO_3)_2$ (solid powder, Tianjin Kemiou Chemical Reagent Co., China), respectively, in the background electrolyte (0.01 mol/L KNO_3 prepared from solid chemical). Working solutions of Pb, Cd and Zn for adsorption kinetics and adsorption isotherm experiments were prepared by diluting the stock solution with 0.01 mol/L KNO_3.

For the adsorption kinetics experiment, 0.10 g of prepared hydroxyapatite-based adsorbent was added to a conical flask containing 100 mL solutions of Pb (340 mg/L), Cd (190 mg/L) or Zn (210 mg/L). The initial pH of these working solutions was adjusted to 5.0 by adding HNO_3 (1.0 mol/L). The conical flask was oscillated at 180 r/min in a horizontal shaker (T = 25 °C, 35 °C) and sampled at different time points (10 min to 48 h). The collected samples were filtered through a 0.45 µm filter and acidified by concentrated HNO_3 for chemical analysis. The concentration of heavy metals in the filtrate was measured by atomic absorption spectrometer (AAS, PerkinElmer PinAAcle 900F, USA). Triplicate experiments were performed for each treatment to calculate the standard deviation.

For the adsorption isotherm experiments, 0.01 g prepared adsorbent was mixed with 10 mL working solutions in 15 mL centrifuge tubes containing Pb (55 to 1200 mg/L), Cd (50 to 550 mg/L), or Zn (10 to 500 mg/L).

The initial pH of the solutions was adjusted to 5.0, and the tubes were oscillated at 180 r/min in a horizontal shaker for 24 h at 25 °C. The solution was centrifuged for 20 min at 2000 r/min, filtered through a 0.45 μm filter and acidified by concentrated HNO_3. The adsorption isotherm was also conducted in a Pb–Cd-Zn multi-metals solution with concentrations of metals ranging from 10 to 400 mg/L. The experiment on pH influence was performed at 25 °C for 24 h, and the pH values of the solution (Pb: 350 mg/L; Zn: 200 mg/L; Cd: 200 mg/L) were adjusted to pH 3.0 and 6.0 by HNO_3 (0.1–1.0 mol/L). The concentrations of Pb, Cd and Zn in the collected aqueous samples were determined by AAS. Triplicate experiments were performed to calculate the standard deviation.

Solid phase characterization

The major chemical compositions of solid samples were determined by X-ray fluorescence spectrometer (XRF, Thermo Fisher Scientific ARL Perform'X 4200, Switzerland). Minerals were measured by powder X-ray diffractometer (XRD, PANalytical Empyrean, The Netherlands), using a Cu Kα (40 kV, 40 mA, λ = 1.5406 Å) monochromatic radiation source in the range of 10–60° and scanning at a step speed of 5°/min. The functional groups of solid samples were determined by the KBr method using Fourier transform infrared spectroscopy (FTIR, Brucker Vertex-70, Germany). Transmission electron microscope (TEM, FEI Tecnai G2 F20 S-Twin, USA) combined with energy dispersive spectroscopy (EDS, EDAX, USA) was applied to characterize the morphology, crystal structure and chemical composition of the prepared adsorbent before and after adsorption of metals. The surface elements of the adsorbent before and after adsorption were analyzed using X-ray photoelectron spectrometry (XPS).

Data fitting for batch experiments

The adsorption capacity (Q_e) was calculated according to the formula described by Mohan et al. (2017):

$$Q_e = \frac{V \cdot (C_0 - C_e)}{M} \quad (1)$$

where Q_e is the adsorption capacity (mg/g); C_0 and C_e denote the concentrations of Pb (mg/L), Cd (mg/L) and Zn (mg/L) at t = 0 and equilibrium, respectively; V (L) refers to the initial volume of the working solution of Pb, Cd and Zn; and M is the weight (g) of the adsorbent.

To investigate the adsorption process and behavior of HMs onto the prepared adsorbent, pseudo-first order kinetics (Eq. 2) and pseudo-second order kinetics (Eq. 3) were used to fit the data according to (Millar et al. 2016):

$$Q_e = Q_t \cdot (1 - e^{-k_1 t}) \quad (2)$$

$$Q_e = \frac{k_2 Q_t^2 t}{1 + k_2 Q_t t} \quad (3)$$

where Q_e and Q_t are the adsorption capacity (mg/g) at equilibrium and time t (min), respectively; k_1 is the pseudo-first-order rate constant (1/min); and k_2 is the pseudo-second-order rate constant (mg/ (g min)).

The Langmuir (Eq. 4) and the Freundlich (Eq. 5) isotherm adsorption models were used to fit the experimental thermodynamic data according to (Millar et al. 2016):

$$Q_e = Q_{max} \cdot \frac{K_L C_e}{1 + K_L C_e} \quad (4)$$

$$Q_e = K_F \cdot C_e^{\frac{1}{n}} \quad (5)$$

where Q_e is the adsorption capacity (mg/g) calculated by model fitting, C_e is the residual concentration of metal ions in the solution at equilibrium (mg/L), Q_{max} is the maximum adsorption capacity (mg/L), K_L is the Langmuir constant, K_F is a constant related to adsorption capacity, and 1/n is an empirical constant related to adsorption strength.

Results and discussion

Characterization of the hydroxyapatite-based adsorbent

The raw phosphate tailing (PT) was primarily composed of CaO (33.0%), MgO (18.0%) and P_2O_5 (5.18%), with loss on ignition (LOI) of 40.2%, and the dominant minerals were dolomite and fluorapatite (Fig. 1 a). The major chemical composition of the hydroxyapatite-based adsorbent prepared from PT (HAP_{PT}) was CaO (36.9%), P_2O_5 (29.6%) and MgO (27.1%), suggesting that MgO existed as impurities based on the stoichiometric ratio of HAP. The dissolution and reprecipitation of phosphate tailing likely introduced MgO into HAP_{PT} because Mg^{2+} began to precipitate at pH ~ 8. The hydroxyapatite (HAP) in HAP_{PT} was characterized by peaks at 2θ values of 25.9°, 31.8°, 32.2°, 32.9° and 49.6° (Li et al. 2017), consistent with that of HAP reference (Fig. 1 a). The FTIR results (Fig. 1 b) showed that both HAP_{PT} and HAP reference presented antisymmetric stretching vibration peaks (1034 cm^{-1}, 1097 cm^{-1}) of PO_4^{3-}, symmetric stretching vibration peak (966 cm^{-1}) and asymmetric variable angle vibration peak (567 cm^{-1}, 603 cm^{-1}) of PO_4^{3-} (Wei et al. 2021). Characteristic peaks of carbonate presented in PT, such as the carbonate antisymmetric stretching peak (1429 cm^{-1}), carbonate out-plane bending peak (876 cm^{-1})

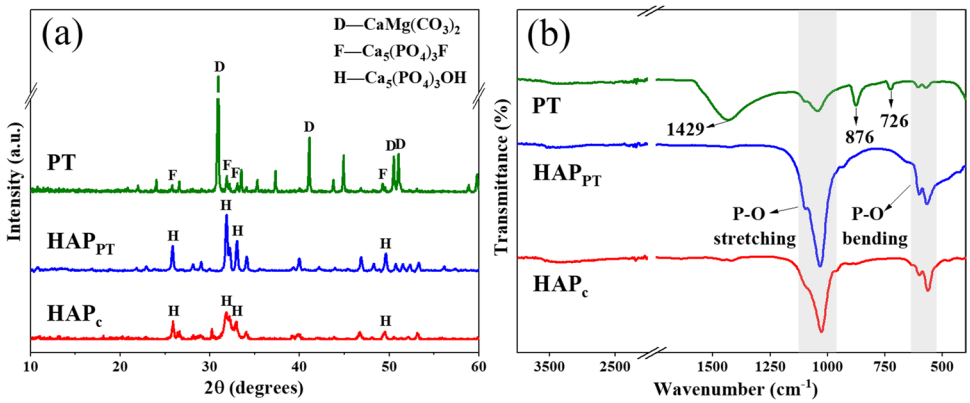

Fig. 1 XRD patterns (**a**) and FTIR spectra (**b**) of phosphate tailing (PT), hydroxyapatite-based adsorbent (HAP_{PT}) and hydroxyapatite reference (HAP_c)

and in-plane bending peak (726 cm^{-1}) (Li et al. 2022a), were not observed in HAP_{PT}. The combined XRD and FTIR results indicated that a hydroxyapatite-based adsorbent was successfully prepared from PT. The yield of this method was approximately 18%, and the content of P_2O_5 in the remaining solids was ~ 0.30%. These results indicated a high recycling rate of phosphorus in phosphate tailing. Additionally, the specific surface area and pore volume of HAP_{PT} were 27.74 m^2/g and 0.51 cm^3/g, respectively.

Adsorption kinetics of Pb, Cd and Zn

In the adsorption kinetic experiments, the adsorption of all metals rapidly increased first, and then slowly reached equilibrium for Pb and Cd, and increased slowly for Zn (Fig. 2). The adsorption kinetics of metals by the prepared HAP_{PT} were similar to previous studies that used HAP as an adsorbent (Liu et al. 2018c; Yuan et al. 2022), in which the adsorption of metals reached equilibrium in hours. The rapid reaction during the initial stage may be related to the changes in concentration of HMs and the adsorption sites (Anirudhan et al. 2009). With increasing HMs concentration, the surface adsorption sites on HAP_{PT} became saturated, and the adsorption gradually decreased. Moreover, the adsorption capacity of metals by HAP_{PT} increased with the temperature increasing from 25 to 35 ℃. The Q_e of Pb and Cd at 25 ℃ were 317.44 and 176.74 mg/kg, respectively, and the Q_e at 35 ℃ increased by 14.1% for Pb and 40.4% for Cd. This result is in agreement with a previous study that the removal efficiency increased by ~ 20% for Pb and Cu when rising the temperature from 25 to 45 ℃ (Liu et al. 2018b). As an exception, the adsorption of Zn gradually increased from initial to 48 h, and the removal efficiency < 50% in the first 6 h.

The calculated kinetic parameters (R^2) showed that both pseudo-first order and pseudo-second order kinetic models can predict the adsorption of Pb and Cd by HAP_{PT} at both temperatures (Table 1), which suggested that physical and chemical adsorption was involved in the processes. The reaction rates of Pb and Cd were higher at 35 ℃ than that at 25 ℃, and the calculated adsorption capacities matched the experimental results well at both temperatures. The low R^2 values of both models for Zn was probably related to the increasing adsorption of Zn with increasing contact time. The higher R^2 of pseudo-second order model may suggest that the overall rate of Zn adsorption was controlled by chemisorption.

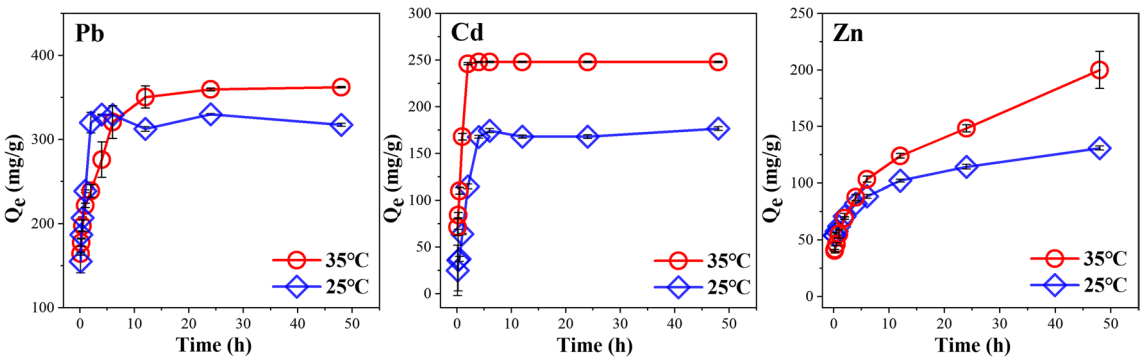

Fig. 2 Adsorption kinetics of Pb, Cd and Zn by HAP_{PT} (T = 25℃, 35 ℃; pH = 5.0)

Adsorption isotherm of Pb, Cd and Zn

Adsorption in mono-metal solution

In mono-metal solutions, the adsorption isotherms varied in different metals (Fig. 3). It was found that the adsorption capacities of metals increased sharply at low initial concentrations. The adsorption capacity of Pb increased rapidly at concentrations < 325 mg/L, then decreased at concentrations ranging from 460 to 685 mg/L, and finally returned to a high level. The adsorption capacity of Cd increased with increasing Cd concentrations and then reached a plateau. The effect of initial concentrations on the adsorption capacity of Cd was similar to but Pb was different from that in previous studies in which Pb increased rapidly and then reached equilibrium (Li et al. 2017; Liu et al. 2018c; Su et al. 2019). The adsorption capacity of Zn increased rapidly at concentrations from 10 to 55 mg/L, slightly fluctuated from 125 to 250 mg/L and then sharply increased again.

The calculated R^2 of fitting showed that the Langmuir model better described the adsorption process of Cd by HAP_{PT} (Table 2), indicating a monolayer adsorption (Mohan et al. 2017). Although both models presented similar R^2 values for Pb and Zn, the negative n value suggested that the Freundlich model was suitable for describing the data. Moreover, the Q_{max} of metals predicted by the Langmuir model was lower than the experimental values.

The adsorption capacities (Q_{max}) of metals by HAP_{PT} decreased in the order of Pb (417.12 mg/g) > Cd (369.14 mg/g) > Zn (117.89 mg/g). In comparison with other

Table 1 Adsorption kinetic parameters of Pb, Cd and Zn on HAP_{PT}

T	Metal	Experimental value	Pseudo-first order			Pseudo-second order		
		Q_e (mg/g)	Q_e (mg/g)	K_1 (min^{-1})	R^2	Q_e (mg/g)	K_2 ($g \cdot mg^{-1} \cdot min^{-1}$)	R^2
25℃	Pb	317.44	327.99	1.77	0.913	344.18	0.94×10^{-2}	0.906
	Cd	176.74	177.03	0.48	0.980	199.35	0.28×10^{-2}	0.927
	Zn	130.94	97.06	3.52	0.440	103.43	3.37×10^{-2}	0.618
35℃	Pb	362.09	355.69	2.56	0.814	346.48	3.10×10^{-2}	0.999
	Cd	248.11	248.64	1.53	0.966	256.35	1.49×10^{-2}	0.770
	Zn	199.96	86.10	2.65	0.518	103.80	2.30×10^{-2}	0.691

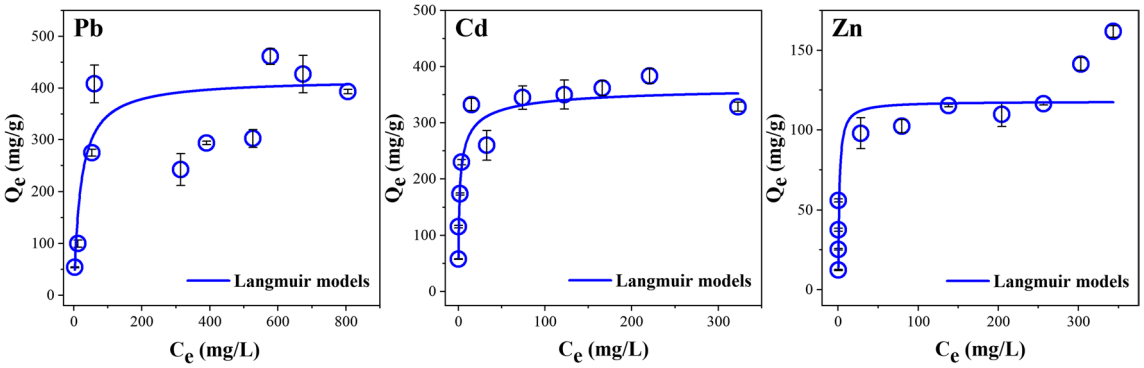

Fig. 3 Adsorption isotherms of Pb, Cd and Zn by HAP_{PT} in mono-metal solution (T = 25℃, pH = 5.0)

Table 2 Freundlich and Langmuir isotherm constants for the adsorption of Pb, Cd and Zn by HAP_{PT}

	Experimental value	Langmuir			Freundlich		
	Q_{max} (mg/g)	Q_{max} (mg/g)	K_L ($L \cdot mg^{-1}$)	R^2	K_F	n	R^2
Pb	461.25	417.12	0.01	0.906	39.73	-0.34	0.960
Cd	383.41	369.14	0.67	0.949	112.10	-0.24	0.772
Zn	161.81	117.89	0.69	0.885	42.00	-0.2	0.985

adsorbents, the adsorption capacities for Pb, Zn and Cd of HAP_{PT} in this study were higher than that of the reported HAP-based materials and other adsorbents (Table 3). For example, the Q_{max} of Cd by HAP_{PT} was 13 times higher than that of natural HAP (Fernane et al. 2008) and HAP synthesized from biological waste (Foroutan et al. 2021). First, the small particle size (< 100 nm) may contribute to the high adsorption capacities. It has been reported that the performance of nanocrystalline HAP in removing Pb and Zn was improved by an order of magnitude compared with that of mesocrystalline HAP (Ibrahim et al. 2020). Second, reactive constitute of MgO in HAP_{PT} may also have an important contribution because dissolution of MgO can increase the solution pH and stimulate HMs to form hydroxide precipitates (Suzuki et al. 2013). The relatively high Q_{max} of metals implied that HAP_{PT} prepared from phosphate tailing is an efficient adsorbent with great potential for the immobilization of Pb, Cd and Zn from soil and water.

Adsorption in multi-metals solution

In the Pb–Cd-Zn multi-metals solution, the adsorption capacity of Pb was substantially higher than that of Cd and Zn, with Q_{max} increasing with increasing C_e for Pb, and Q_{max} fluctuated at approximately 25 mg/g for Cd and Zn (Fig. 4). Compared with the mono-metal solution, the maximum adsorption quantity decreased by 53% for Pb, 93% for Cd and 79% for Zn. These results indicated that Pb was preferentially sequestered by HAP_{PT} in multi-metals solution, consistent with the results for HAP in previous studies (Li et al. 2017; Jing et al. 2018; Zhou et al. 2021). Generally, the competitive adsorption of metals depends on their chemical properties. Zhou et al. (2021) investigated the competitive sorption of Pb, Cu, Zn and Cd in binary-metal solutions and proposed that hydrated radius and electronegativity primarily contribute to the adsorption capacity in multi-metals solution. The adsorption capacity increased with decreasing hydrated radius and increasing electronegativity (Ibrahim et al. 2020). Therefore, Pb was preferentially adsorbed in Pb–Cd-Zn multi-metals solution since it presents a lower hydrated radius (4.01 Å) and higher electronegativity (2.33) than Cd (4.26 Å, 1.69) and Zn (4.30 Å, 1.65). Additionally, the formation of Pb phosphate precipitates may block the surface sites and inhibit the surface complexation of Cd and Zn on HAP (Li et al. 2017).

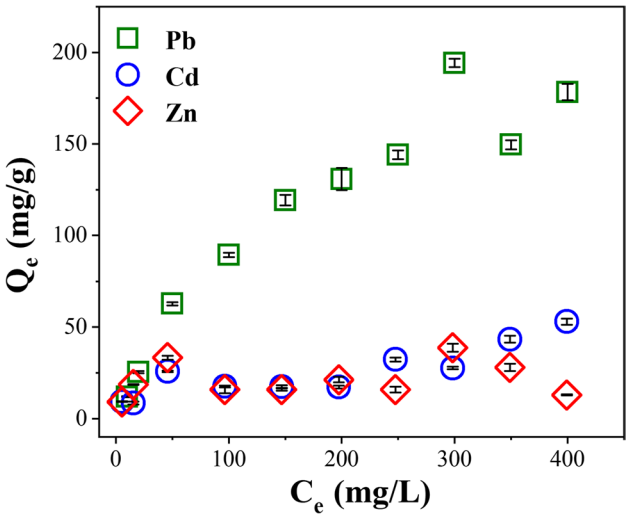

Fig. 4 Adsorption of Pb, Cd and Zn by HAP_{PT} in multi-metals solution (T = 25 °C, pH = 5.0)

Table 3 Comparison of adsorption capacity (Q_{max}) for Pb, Cd and Zn with various adsorbents

	Adsorbent	Q_{max} (mg/g)	Reference
Pb	HAP_{PT}	417.12	This study
	HAP-chitosan	264.42	Guan et al. 2015
	Nanocrystalline HAP	378.62	Wei et al. (2021)
	Graphene oxide	59.50	Gomes et al. (2022)
	Zr-based MOF UiO-66	125.2	Jrad et al. (2022)
	PAHHA	232.48	Duan et al. (2022)
	$MgFe_2O_4$Biochar	198.93	Li et al. (2022b)
	F-HAP	285	Liu et al. (2018b)
Cd	HAP_{PT}	369.14	This study
	Natural HAP	28	Fernane et al. (2008)
	Porous HAP nanosheets	24.9	Su et al. (2019)
	HAP nanoparticles	61.72	Joshi and Manocha (2017)
	HAP-chicken femur	22.94	Foroutan et al. (2021)
	Zr-based MOF UiO-66	69.1	Jrad et al. (2022)
	$MgFe_2O_4$Biochar	195.50	Li et al. (2022b)
	F-HAP	29.2	Liu et al. (2018b)
Zn	HAP_{PT}	147.52	This study
	HAP	37.9	Gibert et al. (2021)
	Ba-HAP	36.62	Sheha (2007)

Effect of pH on adsorption capacity

The adsorption of metals in mono-metal solutions with initial pH values of 3 and 6 is displayed in Fig. 5. The adsorption capacities of Pb and Zn were 189.40 and 115.17 mg/g at pH 3, and were 187.55 and 121.40 mg/kg at pH 6, respectively. These results suggested that HAP_{PT} was an efficient adsorbent for sequestering Pb and Zn in solution with pH ranging from 3 to 6. The adsorption capacity of Cd at pH 6 (206.26 mg/kg) was 45% higher than that at pH 3 (141.81 mg/kg). In a previous study, it showed that nano-hydroxyapatite removed similar quantities of Pb when pH increased from 2 to 5.38, whereas the removal of Cd and Zn at pH 3 is much less than that at pH 6 (Zhou et al. 2021).

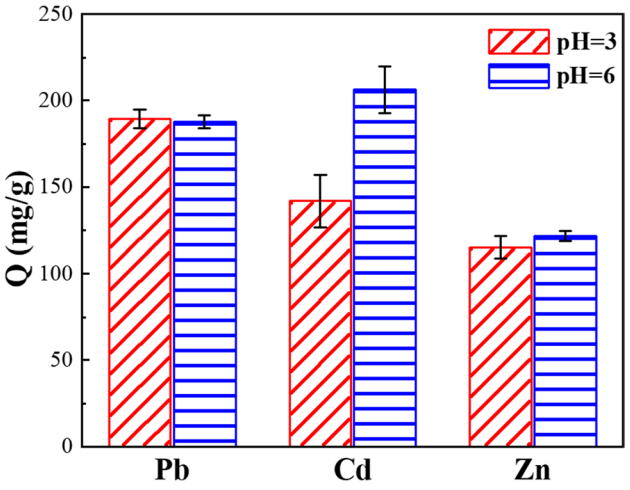

Fig. 5 Effect of initial pH on the adsorption of Pb, Cd and Zn by HAP_{PT}

However, some studies showed that the adsorption capacity of Pb and Cd at pH 6 was approximately 50% higher than that at pH 3 when HAP prepared from flue gas desulphurization gypsum was used as an adsorbent (Yan et al. 2014; Liu et al. 2018b). Generally, the dissolution of HAP, precipitation of metal phosphates and changes in surface charge of HAP under different pH conditions were major factors influencing the adsorption of metals by HAP (Takeuchi and Arai 1990; Hashimoto et al. 2009a; Zhou et al. 2021, 2022). For the HAP_{PT} in this study, the dissolution of MgO in the solution may substantially elevate the initial pH and thus impact the adsorption of metals.

Characterization of HAP_{PT} before and after adsorption

To investigate the immobilizing mechanisms of metals, HAP_{PT} before and after adsorption of 400 mg/L Pb, Cd and Zn was analyzed by TEM-EDS, XRD and XPS. The TEM images of HAP_{PT} showed that there were thin film-like substances with irregular contours (Fig. 6 a) on/around the HAP crystals. Based on the chemical compositions determined by EDS and XRF, these materials could be MgO, which may result from the decomposition of $Mg(OH)_2$ in precipitation during calcination at 800 °C. These results further demonstrated that the prepared material was a HAP-MgO composite. The structure and morphology of HAP_{PT} changed after metal adsorption, indicating the formation of new substances. After adsorption, Pb primarily occurred in short columnar (point 1, atomic proportion of 22.15%) and plate-shaped substances (point 2, atomic proportion of 23.1%) (Fig. 6 b). The chemical composition of these crystals suggested that most Pb resides in phosphates. Cd in the solid was mainly present in long columnar (point 1, atomic proportion of 56.62%) and thin-film materials (point 2, atomic proportion of 51.87%) (Fig. 6 c), and Cd in HAP crystals was not detected by EDS. The Zn in large hydroxyapatite crystals was not detected by EDS (point 1 in Fig. 6 d), but a high content of Zn was observed in nanoparticle aggregates (atomic proportion of 40.01%, point 2 in Fig. 6 d).

To further recognize the newly formed materials after metal adsorption, the minerals in the solid were measured by XRD. For HAP_{PT}-Pb, characteristic peaks of lead phosphate ($Pb_9(PO_4)_6$) were observed in the XRD spectra

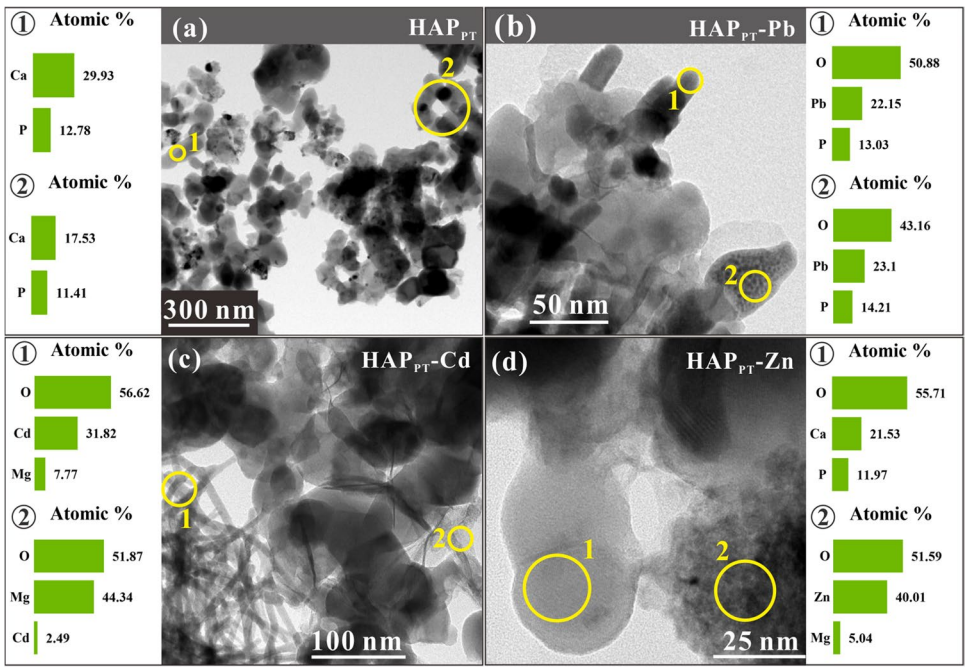

Fig. 6 TEM images and EDS spectra of HAP_{PT} before (**a**) and after adsorption of Pb (**b**), Cd (**c**) and Zn (**d**)

(Fig. 7). Additionally, a characteristic peak at 30.45° was also observed, similar to the results in previous studies (Liu et al. 2018c; Jing et al. 2018), which suggested the presence of $Pb_{10}(PO_4)_6(OH)_2$ or $Pb_xCa_{(10-x)}(PO_4)_6(OH)_2$ (Ibrahim et al. 2020). Characteristic peaks of $Cd(OH)_2$ and $Zn(OH)_2$ were observed in HAP_{PT}-Cd and HAP_{PT}-Zn, respectively (Fig. 7). These results indicated that the metals were immobilized as phosphate and hydroxide precipitates.

The XPS spectra of HAP_{PT} before and after adsorption are plotted in Fig. 8. The occurrence of Pb 4f, Cd 3d and Zn 4p peaks indicated the adsorption of metals on the surface of HAP_{PT}. The two peaks in the XPS spectra of Pb 4f were associated with binding energies of 143.3 eV (Pb $4f_{5/2}$) and 138.4 eV (Pb $4f_{7/2}$) (Fig. 8 b), similar to the result for Pb adsorbed on Fe-doped hydroxyapatite reported in previous studies (Yang et al. 2022), which suggested the precipitation of Pb phosphates and/or isomorphous replacement. Cd has two groups of peaks, Cd $3d_{3/2}$ and Cd $3d_{5/2}$ at binding energies of 411.7 (412.6) and 404.9 (405.8) eV, respectively, indicating the presence of $Cd(OH)_2$ (Ain et al. 2020; Yang et al. 2022). The peaks of Zn $2p_{1/2}$ and Zn $2p_{3/2}$ appeared at 1045.3 and 1022.3 eV, respectively, and the latter likely corresponded to ZnO (Zhou et al. 2021).

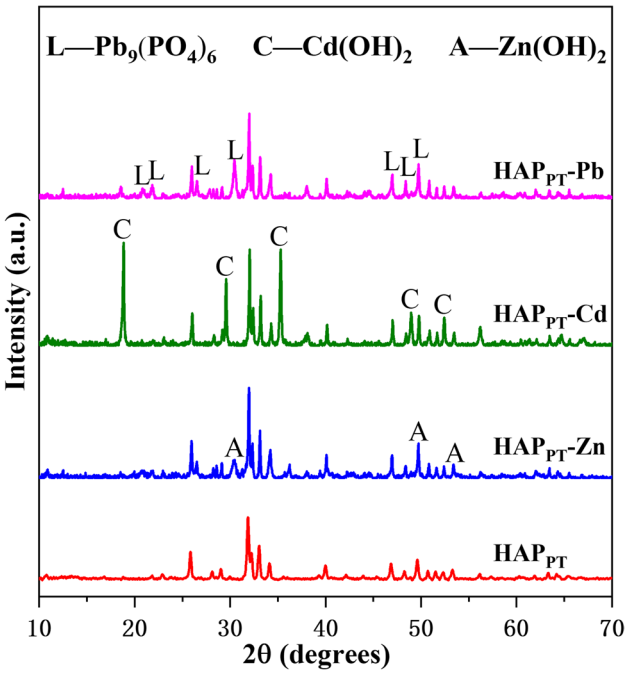

Fig. 7 XRD patterns of HAP_{PT} before and after adsorption of Pb (HAP_{PT}-Pb), Cd (HAP_{PT}-Cd) and Zn (HAP_{PT}-Zn)

Mechanisms of heavy metal immobilization

Generally, potential mechanisms contributing to the immobilization of metals by HAP include ion exchange, surface complexation, dissolution and precipitation (Marchat et al. 2007; Amenaghawon et al. 2022). The combined results of XRD and XPS showed that Pb was primarily immobilized as phosphates. The HAP is stable in basic solution and soluble under acidic conditions such as pH 5 in this study (Eq. 6), and the dissolved $H_2PO_4^-$ released from the dissolution of HAP_{PT} can react with Pb^{2+} to form $Pb_9(PO_4)_6$ or $Pb_{10}(PO_4)_6(OH)_2$ (Eqs. 7 and 8; Cao et al. 2004; Hashimoto et al. 2009b). Additionally, Pb can replace Ca in HAP by ion exchange (Eq. 9; Ibrahim et al. 2020). These reactions can be described by following equations:

$$Ca_{10}(PO_4)_6(OH)_2 + 14H^+ \rightarrow 10Ca^{2+} + 6H_2PO_4^- + 2H_2O \quad (6)$$

$$9Pb^{2+} + 6H_2PO_4^- + 12OH^- \rightarrow Pb_9(PO_4)_6 + 12H_2O \quad (7)$$

$$10Pb^{2+} + 6H_2PO_4^- + 2OH^- \rightarrow Pb_{10}(PO_4)_6(OH)_2 + 12H^+ \quad (8)$$

$$xPb^{2+} + (10-x)Ca^{2+} + 6H_2PO_4^- + 2OH^- \rightarrow Pb_xCa_{(10-x)}(PO_4)_6(OH)_2 + 12H^+ \quad (9)$$

The immobilization mechanisms for Cd and Zn in this study were different from those in previous studies. Foroutan et al. (2021) proposed that the main mechanisms of Cd removal by HAP were dissolution–precipitation and isomorphous substitution. They proposed that soluble phosphate reacted with Cd^{2+} and formed phosphate compounds ($Cd_4H(PO_4)3H_2O$), $Ca_xCd_y(PO_4)_{14}$, $Cd_5(PO_4)_2(OH)_4$ and $Cd(HPO_4{\cdot}H_2O)_2$. Liu et al. (2018c) found that Cd can form complexes rapidly on the surface of HAP-attapulgite composites and then diffuse into the interior of the particles via exchange with Ca. However, in this study, the dominant immobilizing mechanism of Cd and Zn by HAP_{PT} was the precipitation of hydroxides. The MgO in HAP_{PT} was the most important factor contributing to the immobilization of Cd and Zn in solution because the dissolution of MgO released hydroxide ions (Eq. 10; Suzuki et al. 2013). The increase of solution pH consequently stimulate the precipitation of $Cd(OH)_2$ and $Zn(OH)_2$ (Eqs. 11, 12). The function of MgO also explained the high adsorption capacities of Cd and Zn by HAP_{PT}.

$$MgO + H_2O \rightarrow Mg^{2+} + 2OH^- \quad (10)$$

$$Cd^{2+} + 2OH^- \rightarrow Cd(OH)_2 \quad (11)$$

$$Zn^{2+} + 2OH^- \rightarrow Zn(OH)_2 \quad (12)$$

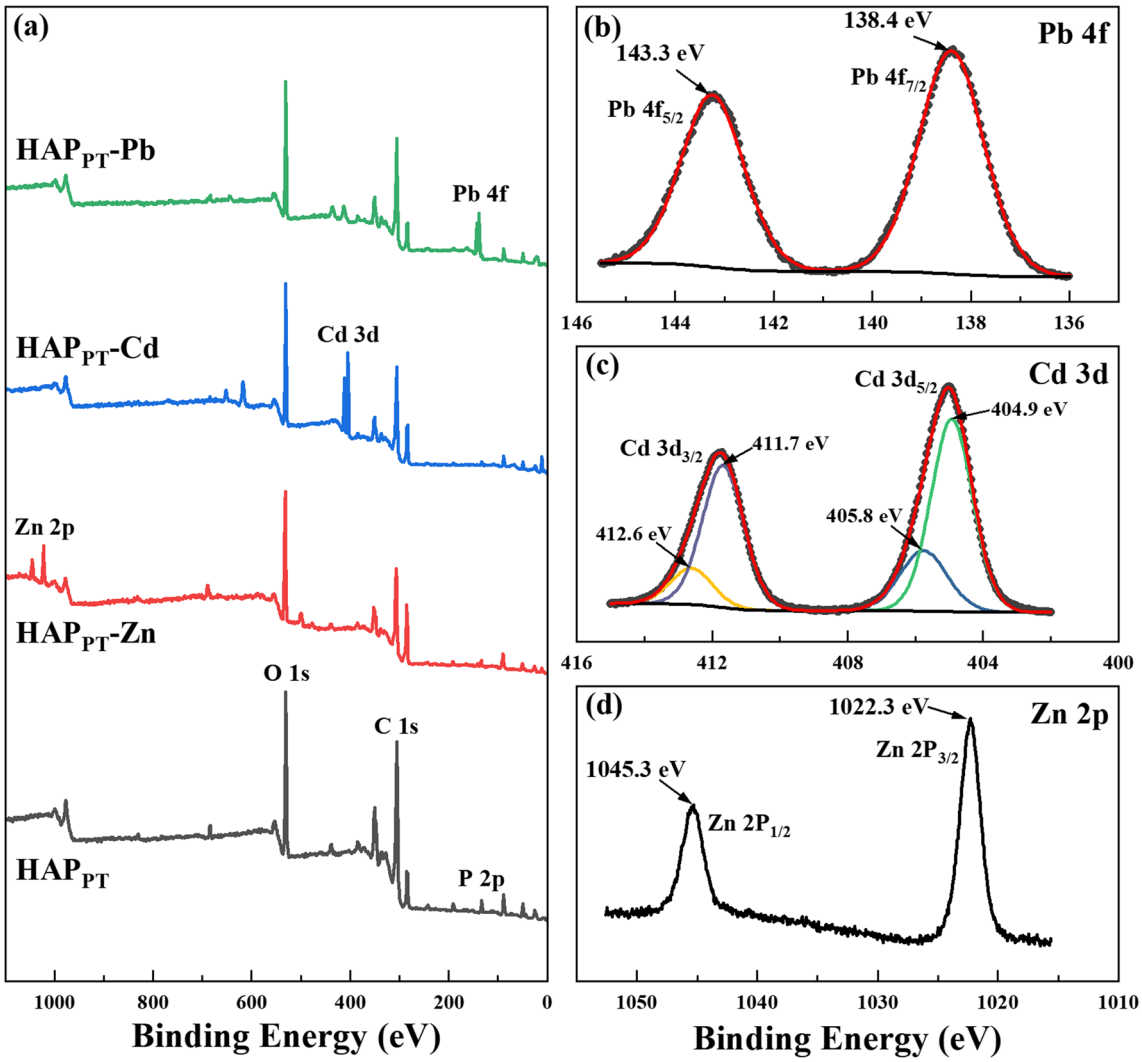

Fig. 8 XPS spectra of Pb 4f, Cd 3d and Zn 2p of HAP_{PT} before (**a**) and after adsorption of Pb (**b**), Cd (**c**) and Zn (**d**)

Conclusion

An efficient hydroxyapatite-based adsorbent composed of hydroxyapatite and MgO was prepared from the recycling of phosphate tailings for immobilizing heavy metal cations from solution in this study. The kinetic experiments showed that the prepared adsorbent can rapidly sequester metals from solution and the adsorption capacities increased with increasing temperature from 25 °C to 35 °C. Moreover, the adsorbent presented high adsorption capacities for Pb, Cd and Zn in mono-metal solution with different pHs, and the adsorption of Cd increased with increasing pH from 3 to 6. In Pb–Cd-Zn multi-metals solution, the adsorption capacities of metals decreased due to competitive adsorption and Pb was preferentially immobilized. The combined results of TEM, XRD and XPS demonstrated that Pb was immobilized by forming phosphate resulting from dissolution of hydroxyapatite, and the formation of hydroxides dominated the immobilization of Cd and Zn due to the dissolution of MgO. From the perspective of clean and sustainable development, the prepared adsorbent can be an alternative for the immobilization of HMs in soil and water.

Author contribution Shanshan Wu: data acquisition, visualization, writing; Yizhang Liu: methodology, editing, supervision, funding acquisition; Lihai Shang: supervision, editing, analysis; Wangwang Zhou: data acquisition, investigation; Yuyang Li: data acquisition; Jing Sun: review, editing; Jianqiu Li: materials; Hui Long: materials; Zengping Ning: review, editing; Chengshuai Liu: review, funding acquisition.

Funding This research was funded by the National Key R&D Programs of China (No. 2020YFC1808501), the Youth Innovation Promotion Association CAS (No. 2021399), and the complementary fund from the Department of Science and Technology of Guizhou Province.

Data availability The datasets used or analyzed in the current study are available from the corresponding author on reasonable request.

Declarations

Ethical approval Not applicable.

Consent to participate Not applicable.

Consent to publish Not applicable.

Competing interests The authors declare no competing interests.

References

Ain QU, Zhang H, Yaseen M, Rasheed U, Liu K, Subhan S, Tong Z (2020) Facile fabrication of hydroxyapatite-magnetite-bentonite composite for efficient adsorption of Pb(II), Cd(II), and crystal violet from aqueous solution. J Clean Prod 247:119088

Amar H, Benzaazoua M, Elghali A, Hakkou R, Taha Y (2022) Waste rock reprocessing to enhance the sustainability of phosphate reserves: A critical review. J Clean Prod 381:135151

Amenaghawon AN, Anyalewechi CL, Darmokoesoemo H, Kusuma HS (2022) Hydroxyapatite-based adsorbents: Applications in sequestering heavy metals and dyes. J Environ Manag 302:113989

Anirudhan TS, Jalajamony S, Suchithra PS (2009) Improved performance of a cellulose-based anion exchangerwith tertiary amine functionality for the adsorption of chromium(VI) from aqueous solutions. Colloids Surf A 335:107–113

Ashrit SS, Chatti RV, Sarkar S (2020) Synthesis and characterization of hematite based calcium rich hydroxyapatite-A nano material from LD slag fines. J Environ Chem Eng 8:103581

Asri SE, Laghzizil A, Coradin T, Saoiabi A, Alaoui A, M'hamdi R (2010) Conversion of natural phosphate rock into mesoporous hydroxyapatite for heavy metals removal from aqueous solution. Colloid Surface A 362:33–38

Ayari J, Barbieri M, Barhoumi A, Boschetti T, Braham A, Dhaha F, Charef A (2023) Trace metal element pollution in media from the abandoned Pb and Zn mine of Lakhouat, Northern Tunisia. J Geochem Explor 247:107180

Azhar U, Ahmad H, Shafqat H, Babar M, Munir HMS, Sagir M, Arif M, Hassan A, Rachmadona N, Rajendran S, Mubashir M, Khoo KS (2022) Remediation techniques for elimination of heavy metal pollutants from soil: A review. Envrion Res 214:113918

Bolan N, Kunhikrishnan A, Thangarajan R, Kumpiene J, Park J, Makino T, Kirkham MB, Scheckel K (2014) Remediation of heavy metal(loid)s contaminated soils – To mobilize or to immobilize? J Hazard Mater 266:141–166

Cao X, Ma LQ, Rhue DR, Appel CS (2004) Mechanisms of lead, copper, and zinc retention by phosphate rock. Envrion POLLUT 131:435–444

Cidu R, Dadea C, Desogus P, Fanfani L, Manca PP, Orru G (2012) Assessment of environmental hazards at abandoned mining sites: A case study in Sardinia, Italy. Appl Geochem 27:1795–1806

Duan G, Cao Z, Zhong H, Ma X, Wang S (2022) Highly efficient poly(6-acryloylamino-N-hydroxyhexanamide) resin for adsorption of heavy metal ions. J Environ Mang 308:114631

Fang Y, Zhao G, Dai W, Ma L, Ma N (2017) Enhanced adsorption of rubidium ion by a phenol@MIL-101(Cr) composite material. Micro Por Mesopor Mat 251:51–57

Fernane F, Mecherri MO, Sharrock P, Hadioui M, Lounici H, Fedoroff M (2008) Sorption of cadmium and copper ions on natural and synthetic hydroxyapatite particles. Mater Charact 59:554–559

Foroutan R, Peighambardoust SJ, Hosseini SS, Akbari A, Ramavandi B (2021) Hydroxyapatite biomaterial production from chicken (femur and beak) and fishbone waste through a chemical less method for Cd^{2+} removal from shipbuilding wastewater. J Hazard Mater 413:125428

Gibert O, Valderrama C, Martinez MM, Darbra RM, Moncunill JO (2021) Hydroxyapatite coatings on calcite powder for the removal of heavy metals from contaminated water. Water 13:1493

Gomes BFML, de Araujo CMB, do Nascimento BF, de Luna Freire EMP, Sobrinho MADM, Carvalho MN (2022) Synthesis and application of graphene oxide as a nanoadsorbent to remove Cd(II) and Pb(II) from water: adsorption equilibrium, kinetics, and regeneration. Environ Sci Pollut Res 29:17358–17372

Gu K, Chen B, Yan P, Wang J (2022) Recycling of phosphate tailings and acid wastewater from phosphorus chemical industrial chain to prepare a high value-added magnesium oxysulfate cement. J Clean Prod 369:133343

Guan J-J, Ke Q-F, Lei Y, Chen W, Zhang C-Q (2015) Fabrication of hydroxyapatite/chitosan porous materials for Pb(II) removal from aqueous solution. RSC ADV 5:25462-25470

Hashimoto Y, Taki T, Sato T (2009a) Sorption of dissolved lead from shooting range soils using hydroxyapatite amendments synthesized from industrial byproducts as affected by varying pH conditions. J Environ Manag 90:1782–1789

Hashimoto Y, Takaoka M, Oshita K, Tanida H (2009b) Incomplete transformations of Pb to pyromorphite by phosphate-induced immobilization investigated by X-ray absorption fine structure (XAFS) spectroscopy. Chemosphere 76:616–622

Ibrahim M, Labaki M, Giraudon JM, Lamonier JF (2020) Hydroxyapatite, a multifunctional material for air, water and soil pollution control: A review. J Hazard Mater 383:121139

Ivanets AI, Kitikova NV, Shashkova IL, Roshchina MY, Srivastava V, Sillanpää M (2019) Adsorption performance of hydroxyapatite with different crystalline and porous structure towards metal ions in multicomponent solution. J Water Process Eng 32:100963

Jing N, Zhou AN, Xu QH (2018) The synthesis of super-small nano hydroxyapatite and its high adsorptions to mixed heavy metallic ions. J Hazard Mater 353:89–98

Joshi P, Manocha S (2017) Sorption of cadmium ions onto synthetic hydroxyapatite nanoparticles. Materials today: Proceedings 4:10460–10464

Jrad A, Damacet P, Yaghi Z, Ahmad M, Hmadeh M (2022) Zr-Based Metal-Organic Framework Nanocrystals for Water Remediation. ACS Appl Nano Mater 5:10795–10808

Kan X, Dong Y, Feng L, Zhou M, Hou H (2021) Contamination and health risk assessment of heavy metals in China's lead-zinc mine tailings: A meta-analysis. Chemosphere 267:128909

Lee SS, Lim JE, Abd El-Azeem SAM, Choi B, Oh SE, Moon DH, Ok YS (2013) Heavy metal immobilization in soil near abandoned mines using eggshell waste and rapeseed residue. Environ Sci Pollut Res 20:1719–1726

Li H, Guo X, Ye X (2017) Screening hydroxyapatite for cadmium and lead immobilization in aqueous solution and contaminated soil: The role of surface area. J Environ Sci 52:141–150

Li J, Nie G, Li J, Zhu Z, Wang Z (2022a) Flotation separation of quartz and dolomite from collophane using sodium N-dodecyl-β-amino propionate and its adsorption mechanism. Colloids Surf A 641:128586

Li A, Xie H, Qiu Y, Liu L, Lu T, Wang W, Qiu G (2022b) Resource utilization of rice husk biomass: Preparation of MgO flake-modified biochar for simultaneous removal of heavy metals from aqueous solution and polluted soil. Environ Pollut 310:11986

Liu S, Tian S, Li K, Wang L, Liang T (2018a) Heavy metal bioaccessibility and health risks in the contaminated soil of an abandoned, small-scale lead and zinc mine. Environ Sci Pollut Res 25:15044–15056

Liu Y, Yan Y, Seshadri B, Qi F, Xu Y, Bolan N, Zheng F, Sun X, Han W, Wang L (2018b) Immobilization of lead and copper in aqueous solution and soil using hydroxyapatite derived from flue gas desulphurization gypsum. J Geochem Explor 184:239–246

Liu G, Li Z, Xu L, Xu X, Huang Q, Zeng Y, Wen M (2018c) The dynamics and adsorption of Cd (II) onto hydroxyapatite attapulgite composites from aqueous solution. J Sol-Gel Sci Technol 87:269–284

Luo Z, Ma S, Hu S, Chen D (2017) Towards the sustainable development of the regional phosphorus resources industry in China: a system dynamics approach. Resour Conserv Recycl 126:186–197

Marchat D, Bernache-Assollant D, Champion E (2007) Cadmium fixation by synthetic hydroxyapatite in aqueous solution - Thermal behaviour. J Hazard Mater 139:453–460

Marzouk ER, Chenery SR, Young SD (2013) Predicting the solubility and lability of Zn, Cd, and Pb in soils from a minespoil-contaminated catchment by stable isotopic exchange. Geochim Cosmochim Acta 123:1–16

Millar GJ, Miller GL, Couperthwaite SJ, Papworth S (2016) Factors influencing kinetic and equilibrium behaviour of sodium ion exchange with strong acid cation resin. Sep Purif Technol 163:79–91

Mohan S, Kumar V, Singh DK, Hasan SH (2017) Effective removal of lead ions using graphene oxide-MgO nanohybrid from aqueous solution: Isotherm, kinetic and thermodynamic modeling of adsorption. J Environ Chem Eng 5:2259–2273

Moukannaa S, Loutou M, Benzaazoua M, Vitola L, Alami J, Hakkou R (2018) Recycling of phosphate mine tailings for the production of geopolymers. J Clean Prod 185:891–903

Nayak A, Bhushan B (2021) Hydroxyapatite as an advanced adsorbent for removal of heavy metal ions from water: Focus on its applications and limitations. Mater Today: Proc 46:11029–11034

Sawada M, Sridhar K, Kanda Y, Yamanaka S (2021) Pure hydroxyapatite synthesis originating from amorphous calcium carbonate. Sci Rep 111(11):1–9

Sheha RR (2007) Sorption behavior of Zn (II) ions on synthesized hydroxyapatites. J Colloid Interf Sci 310:18–26

Su Y, Wang J, Li S, Zhu J, Liu W, Zhang Z (2019) Self-templated microwave-assisted hydrothermal synthesis of two-dimensional holey hydroxyapatite nanosheets for efficient heavy metal removal. Environ Sci Pollut Res 26:30076–30086

Suzuki T, Nakamura A, Niinae M, Nakate H, Fujii H, Tasaka Y (2013) Lead immobilization in artificially contaminated kaolinite using magnesium oxide-based materials: Immobilization mechanisms and long-term evaluation. Chem Eng J 232:380–387

Takeuchi Y, Arai H (1990) Removal of coexisting Pb^{2+}, Cu^{2+} and Cd^{2+} ions from water by addition of hydroxyapatite powder[J]. J Chem Eng Jpn 23(1):75–80

Tian N, Wu J, Wang J, Dai W (2019) Development of a Novel Core-Shell Magnetic Fe3O4@CMC@ZIF-8-OH Composite with Outstanding Rubidium-Ion Capacity. J Chem Eng Data 64:5716–5724

Vareda JP, Valente AJM, Duraes L (2019) Assessment of heavy metal pollution from anthropogenic activities and remediation strategies: A review. J Environ Mang 246:101–118

Wei W, Han X, Shao Y, Xie W, Zhang Y, Yao Y, Zhao W, Han R, Li S, Zhang Y, Zheng C (2021) Comparing the effects of humic acid and oxalic acid on Pb(II) immobilization by a green synthesized nanocrystalline hydroxyapatite. Chemosphere 285:131411

Yan Y, Dong X, Sun X, Sun X, Li J, Shen J, Han W, Liu X, Wang L (2014) Conversion of waste FGD gypsum into hydroxyapatite for removal of Pb^{2+} and Cd^{2+} from wastewater. J Colloid Inter Sci 429:68–76

Yang Z, Gong H, He F, Repo E, Yang W, Liao Q, Zhao F (2022) Iron-doped hydroxyapatite for the simultaneous remediation of lead-, cadmium- and arsenic-co-contaminated soil. Environ Pollt 312:119953

Yuan M, Gu Z, Xia S, Zhao J, Wang X (2022) In-situ remediation of zinc contaminated soil using phosphorus recovery product: Hydroxyapatite/calcium silicate hydrate (HAP/C–S–H). Chemosphere 286:131664

Zhou C, Wang X, Wang Y, Song X, Fang D, Ge S (2021) The sorption of single- and multi-heavy metals in aqueous solution using enhanced nano-hydroxyapatite assisted with ultrasonic. J Environ Chem Eng 9:105240

Zhou C, Song X, Wang Y, Wang H, Ge S (2022) The sorption and short-term immobilization of lead and cadmium by nano-hydroxyapatite/biochar in aqueous solution and soil. Chemosphere 286:131810